ORIGINAL RESEARCH PAPER



Wideband IMD3 suppression through negative baseband impedance synthesis

William Sear 🗅

Taylor W. Barton [©]

Department of Electrical, Computer and Energy Engineering, University of Colorado Boulder, Boulder, CO, USA

Correspondence

William Sear, Department of Electrical, Computer and Energy Engineering, University of Colorado Boulder, Boulder, CO, USA. Email: william.sear@colorado.edu

Funding information

National Science Foundation, Grant/Award Number: 1846507

Abstract

This article presents a power amplifier (PA) linearisation approach based on synthesising a negative impedance termination at the baseband frequency. Negative baseband termination has been previously shown to suppress intermodulation distortion (IMD) products in power amplifiers. Here, this effect is synthesised using a passive feedback network between the drain and gate bias paths of the PA, so that the IMD is suppressed without an increase in the system complexity. The design targets IMD3 suppression at the PA's 3-dB compression point (P3dB), enabling linear operation into compression, therefore, resulting in improved device utilisation and efficiency. Based on simulation of the feedback response over a 1-200 MHz frequency range, a network topology is designed that provides both the bias structure and the appropriate transfer function for IMD3 suppression, demonstrating the first reported practical structure to realize this behaviour over a wide range of baseband frequencies. Two different transfer functions are implemented and compared in performance to the nominal design case with standard baseband terminations. Due to the feedback nature of the approach, stability is also addressed. The 2.14-GHz proof-ofconcept prototype with feedback exhibits up to 9.5 dB suppression of the two-tone IMD3 over 10-150 MHz tone spacing, without reducing the CW performance of the PA.

1 | INTRODUCTION

Next-generation RF and microwave power amplifiers (PAs) will require the ability to operate on high instantaneous bandwidth signals while maintaining both high efficiency and linearity. Conventional linear classes of PAs tend to exhibit improved linearity at output power back-off, but this operating point corresponds to low efficiency. The standard approach to break this efficiency-linearity trade-off is to operate closer to power compression and use digital pre-distortion (DPD) to correct non-linearities. This approach is increasingly challenging as the PA nears compression. Likewise, DPD becomes a less attractive solution for high instantaneous bandwidths due to the challenges of bandwidth scaling in the digital domain. Analogue linearisation techniques, on the other hand, are useful in applications without access to digital baseband signals, such as in the repeaters [1, 2], or when the system complexity makes sampling of individual PA outputs challenging, as in the phased array or MIMO systems [3-5]. Therefore, there is interest in developing an analogue

linearisation technique that is able to scale with increasing carrier frequencies and fractional bandwidth, and that does not increase the associated operating complexity of the PA [6]. The architecture presented in this article, shown in Figure 1, achieves low complexity by implementing analogue linearisation through out-of-band feedback between the drain and gate of the device.

Several analogue linearisation techniques for PAs have been proposed and investigated. One of the oldest techniques is the feedforward amplifier architecture, in which the PA and the error amplifier are used to generate a 180° out-of-phase copy of the third-order intermodulation (IM3) products that cancel the IM3 products at the output [7]. While feedforward amplifiers exhibit exceptional linearity, they struggle to operate at high efficiencies, for example one 'high efficiency' feedforward amplifier reports 10% PAE in compression [8]. Alternatively, IM2 feedforward architectures introduce an auxiliary path to cancel the IM3 products. In this case, the common-mode IM3 response of a cascode amplifier is passed to its output, where the non-linear

This is an open access article under the terms of the Creative Commons Attribution License, which permits use, distribution and reproduction in any medium, provided the original work is properly cited

^{© 2021} The Authors. IET Microwaves, Antennas & Propagation published by John Wiley & Sons Ltd on behalf of The Institution of Engineering and Technology.

transconductance response is cancelled out, thus suppressing the IM3 products [9].

Lower-complexity alternatives include analogue predistortion through diode structures providing a gain-expansion characteristic [10, 11], a technique commonly applied to the travelling wave tube amplifiers (TWTAs) [12, 13]. Conventional single-ended amplifiers can also be made linear through selection of the amplifier's bias point to operate in a 'sweet spot' [14, 15]. Third order intermodulation (IMD3) sweet spots, as seen in Figure 2, are selected by choice of the bias point and impedance terminations such that the third-order and higher odd order distortion terms of the device channel current (small signal or 'weak' non-linear distortion mechanisms) interact with the distortion produced by the device clipping effects (large signal or 'strong' non-linear distortion mechanisms) to produce a minimum in the overall IM3 [16]. Since the underlying mechanisms are power-dependent, these sweet spots occur over a limited range of output power levels, and an efficiencylinearity compromise [17] is apparent.

It is well known that non-zero baseband impedance in the bias line of an amplifier will induce self-modulation effects that

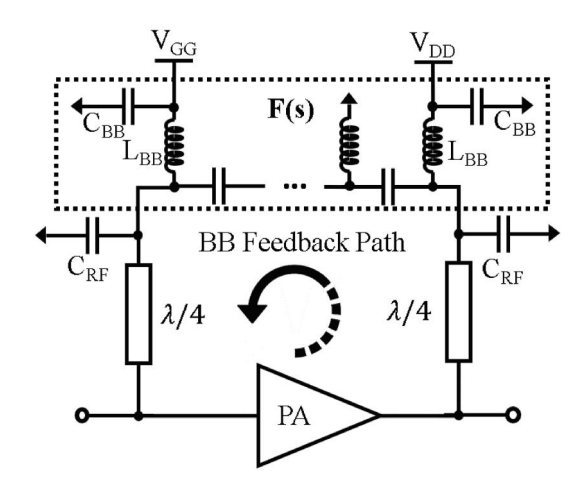


FIGURE 1 Block diagram of the proposed architecture, in which a negative IF impedance is synthesised at the drain through feedback. By appropriately selecting the characteristics of the transfer function F(s), IMD3 tones can be suppressed at an arbitrary output power level

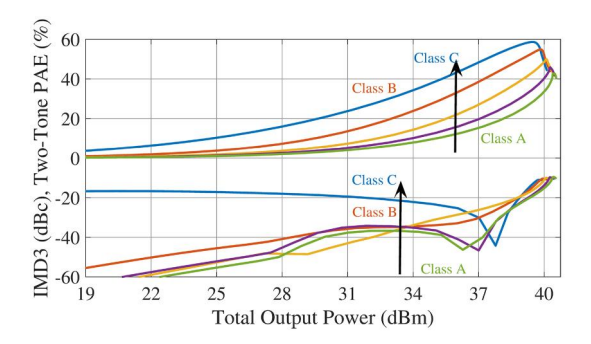


FIGURE 2 Measured IMD3 and PAE of the prototype 2.14-GHz PA without feedback operated under two-tone excitation with 10 MHz spacing over bias conditions between class A and class C. The efficiency-linearity trade-off and bias-dependence of sweet spot generation are apparent

degrade linearity [14–16, 18–29]. In [27], it was demonstrated that presenting a negative baseband impedance significantly improves the IMD product suppression compared with a short-circuit termination. These results indicate that IMD products resulting from third-order non-linearities (IMD3) can be effectively suppressed through analogue techniques focussed on controlling the impedance presented at the signal baseband. This negative impedance improvement (reduction) in IMD3 is demonstrated experimentally in [27] using an active baseband load-pull test bench.

This article presents a linearity enhancement technique that realises a negative baseband impedance without the need for an external signal source. In the proposed approach, the baseband tones generated at the transistor drain are fed back to the gate so that they are amplified by the low-frequency gain of the device; thus synthesising a negative baseband-frequency impedance at the drain of the transistor, whereas in the previous studies this baseband tone injection has been accomplished using external generators [27]. In this work, a simple passive network is introduced and the transistor gain is re-used for based amplification. This technique was originally proposed by Hu et al. in 1986 [25] for a GaAs amplifier, but subsequent development has been limited.

The low-frequency feedback path is analogous to the 'reflex' amplifier concept used in tube amplifiers in the early days of wireless communication [30], except the signal is not demodulated before being fed back into the PA. The feedback network can therefore be incorporated into the bias structure, for example at the end of a conventional quarter-wave line network, as shown in Figure 1. Thus, the baseband IMD correction minimally perturbs the RF performance of the PA and does not substantially increase its cost, size, weight or power consumption.

The goal of this work is to artificially generate a local minimum in the IMD3 response. Focus is laid on linearising the PA, that is, suppressing IMD3, at its P3dB point, where conventional techniques suffer and efficiency is high. The P3dB point was also selected to demonstrate that the technique can be effective in the regions of operation where distortion is dominated by the clipping effects. Compared with previous demonstrations, including the proof-of-concept work in [31] in which a single IMD3 tone in a UHF power amplifier was suppressed for a specific tone spacing only. In this work, the technique is extended to address both the upper and the lower IMD3 tones across tone spacings spanning 10–200 MHz. This article presents additional development of the theoretical performance of the proposed technique, along with an analysis of stability.

This article is organised as follows. Section 2 describes the distortion contributions from the transistor's non-linear drain-source capacitance and non-linear transconductance. Section 3 presents baseband feedback theory as a method to control the transistor's weak nonlinear effects in a class-AB PA. The associated stability response of the baseband feedback path is discussed in Section 4. In Section 5, the design of a class-AB amplifier with a baseband feedback path that minimises distortion is developed. Section 6 discusses the results of the

class-AB amplifier with baseband feedback. Section 7 concludes the article.

2 | WEAK NON-LINEAR DISTORTION MECHANISMS

The weak non-linear response of a transistor, that is, excluding the clipping effects, can be described in terms of the secondand third-order variations in transconductance g_m , conductance g_d , and output capacitance C_{ds} as a function of frequency and power as described in (1).

$$i_{nl} = \tilde{G}_2 V^2(t) + \tilde{G}_3 V^3(t)$$

+
$$\frac{\partial}{\partial t} \left(\tilde{C}_{ds,2} V^2(t) + \tilde{C}_{ds,3} V^3(t) \right)$$
(1)

Here, G_n and $C_{ds,n}$ represent the nth derivative of the non-linear transconductance and non-linear drain to source capacitance, respectively. Non-linear conductance is a particularly dominant effect in GaN devices; for example, the derivative terms for the CGH27015 F transistor used in this work, extracted from dc simulation of a large-signal model [32], are shown in Figure 3. The model described in [33] is used in this work because it has the additional modelling of the IF response compared with the manufacturer-provided model, although this is not the intended application of the embedding model. The information available from simulation, even with this model, is not sufficient for an accurate prediction of the IMD3 response of the device under compression conditions. Therefore, simulation results are used only to approximate the trends in the upper and lower IMD3 tones.

The theory relating the baseband impedance termination at the drain of the transistor and the resulting intermodulation product strength under two-tone excitation are described in detail in [16, 21, 26]. These articles model the IMD3 tone power using a Wiener non-linear model which uses transfer coefficients (H_1 , H_2 , H_3 , ...) that are functions of the lower order transfer coefficients, the drain impedance, and the channel and parasitic capacitance non-linearities. To model the

behaviour of the third-order IMD products. the Wiener non-linear model is truncated to three terms which are given by (2)-(4) repeated from [21].

$$H_{1}(\omega) = \frac{1}{Y_{L}(\omega)} = Z_{L}(\omega)$$

$$H_{2}(\omega_{a}, \omega_{b}) = -Z_{L}(\omega_{a} + \omega_{b}) \times [\tilde{G}_{2} + j(\omega_{a} + \omega_{b})\tilde{C}_{ds,2}]$$

$$\times [H_{1}(\omega_{a})H_{1}(\omega_{b})]$$

$$(3)$$

$$H_{3}(\omega_{a}, \omega_{b}, \omega_{c}) = \frac{-Z_{L}(\omega_{a} + \omega_{b} + \omega_{c})}{6}$$

$$\left\{ 2[\tilde{G}_{2} + j(\omega_{a} + \omega_{b} + \omega_{c})\tilde{C}_{ds,2}][H_{1}(\omega_{a})H_{2}(\omega_{b}, \omega_{c})$$

$$+ H_{1}(\omega_{b})H_{2}(\omega_{a}, \omega_{c}) + H_{1}(\omega_{c})H_{2}(\omega_{b}, \omega_{a})]$$

$$+ 6[\tilde{G}_{3} + j(\omega_{a} + \omega_{b} + \omega_{c})\tilde{C}_{ds,3}][H_{1}(\omega_{a})H_{1}(\omega_{b})H_{1}(\omega_{c})] \right\}$$

$$(4)$$

In (2)-(4), the frequency terms ω_a , ω_b , and ω_c represent temporary variables which will be substituted with appropriate fundamental frequency terms to evaluate the resulting IMD3 products. In this work, because the focus is on the two-tone evaluation of linearity, $\omega_1 = \omega_0 - \omega_\Delta/2$ and $\omega_2 = \omega_0 + \omega_\Delta/2$ are used to represent the two fundamental-frequency tones. Following [21], the lower IMD3 term is found by evaluating $H_3(\omega_1, \omega_1, -\omega_2)$ and the upper IMD3 tone by evaluating $H_3(\omega_2, \omega_2, -\omega_1)$.

$$H_{3}(\omega_{1}, \omega_{1}, -\omega_{2}) = \frac{-Z_{L}(2\omega_{1} - \omega_{2})}{6}$$

$$\left\{2[\tilde{G}_{2} + j(2\omega_{1} - \omega_{2})\tilde{C}_{ds,2}] \times [2Z_{L}(\omega_{1})H_{2}(\omega_{1}, -\omega_{2}) + Z_{L}(-\omega_{2})H_{2}(\omega_{1}, \omega_{1})] + 6[\tilde{G}_{3} + j(2\omega_{1} - \omega_{2})\tilde{C}_{ds,3}][2Z_{L}(\omega_{1})Z_{L}(-\omega_{2})]\right\}$$
(5)

Although there is not an exact correlation between the two-tone IMD3 products and the linearity metrics used in applications, such as the adjacent channel power ratio (ACPR)

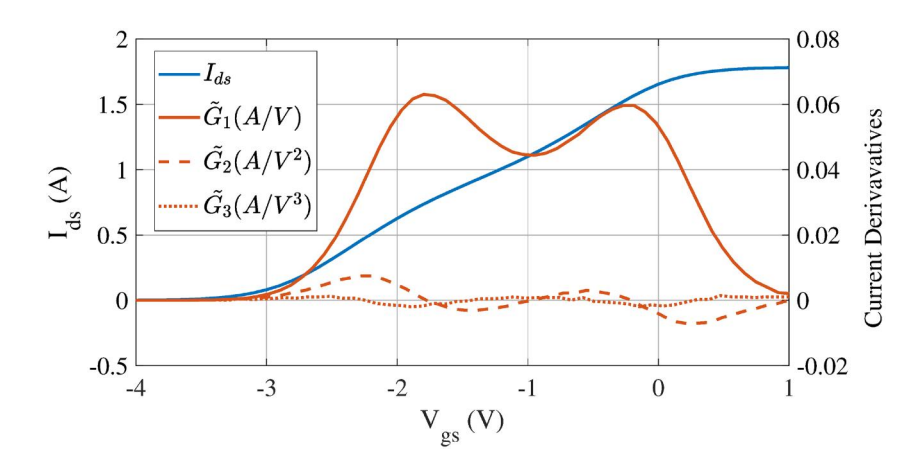


FIGURE 3 Transistor I_{ds} - V_{gs} dc transfer function and first three derivatives. The third-order derivative (G_3) is proportional to the dominant weak non-linearity

[34], this method is useful in system analysis and is adopted here. A single term of interest that comprises the central multiplicative term ξ is identified:

$$\xi = 2Z_L(\omega_1)H_2(\omega_2, -\omega_1) + Z_L(-\omega_1)H_2(\omega_1, \omega_1)$$
 (6)

The ξ expression includes two lower-order transfer functions (H_2) that are functions of the impedances presented to the transistor: one a function of the baseband impedance and the other a function of the second harmonic impedance:

$$H_2(\omega_1, -\omega_2) = -Z_L(\omega_1 - \omega_2) \times [\tilde{G}_2 + j(\omega_1 - \omega_2)\tilde{C}_{ds,2}] \times [H_1(\omega_1)H_1(-\omega_2)]$$
(7)

$$H_{2}(\omega_{1},\omega_{1}) = -Z_{L}(2\omega_{1}) \times [\tilde{G}_{2} + j(2\omega_{1})\tilde{C}_{ds,2}][Z_{L}(\omega_{1})]^{2}$$
(8)

An equivalent expression can also be derived for the upper IMD3 tone with the key difference that the upper IMD3 tone is dependent on its second harmonic impedance, but the same baseband impedance as the lower IMD3 tone.

From the ξ expression, it can be seen that to suppress IMD3 in conventional amplifier modes (Class-A, AB, B) in which the second harmonic frequencies are terminated in a short circuit, the IF baseband should also be terminated in a short circuit up to the maximum modulation frequency. Furthermore, a negative IF impedance can significantly improve the IMD3 suppression compared with a short one [27]. As the PA begins to compress, both weak and strong nonlinearities are present, suggesting that in limited compression (where the efficiency is high and linearity is low) the introduction of a negative impedance could allow the PA to operate in the high-efficiency power region while maintaining sufficient linear response.

3 | BASEBAND FEEDBACK LINEARIZATION

In this work, a negative baseband impedance is synthesised without requiring an external signal source. This is accomplished by recognising that the PA under the test already generates an intermodulation term at the baseband frequency. To realise a negative impedance, the baseband tone can then be fed back from the drain of the amplifier to the gate of the amplifier, so that the tone can be amplified through the transistor. This feedback path transfer function must have the appropriate amplitude and phase shift to suppress IMD3 across a broad range of frequencies. The feedback transfer function, defined as a voltage ratio and shown as F(s) in Figure 1, is defined in terms of arbitrary frequency-dependent amplitude and phase as:

$$F(s) = A_F(s)e^{j\theta_F(s)} \tag{9}$$

Because of the large number of interrelated device parameters determining the optimum transfer function F(s), its parameters A_F and θ_F are found through simulation of a feedback path placed between the gate and drain of the PA described in Section 5.

Figure 4 shows the simulated upper and lower IMD3 tone response to the feedback path for tone spacings from 1 to 200 MHz as $A_F(s)$ and $\theta_F(s)$ are varied with a baseband diplexer element (dc blocking capacitor and dc feed inductor) present to bias the amplifier as it will be in practice. The transistor is operated with a class AB bias ($I_Q = 150$ mA) in both the simulation and in the experimental system. The benchmark case in which the baseband is terminated with a short circuit, with no second stage baseband inductor (L_{BB} in Figure 1) is used as a reference. The contours represent values in the F(s) plane for which the IMD3 tone at P3dB is improved (i.e. IMD3 tone power is reduced) compared with the shorted IF case. The markers indicate the values for F(s) corresponding to the best possible suppression of the upper or lower IMD3 tone power (i.e. the optimum feedback response at that frequency).

Based on the information in Figure 4, a transfer function F(s) is constructed as shown in Figure 5 where the diplexer element used to simulate the feedback path is de-embedded. This figure plots the optimal (as predicted by large-signal simulation) amplitude and phase response across the frequency to minimise either the upper or lower tone, and the resulting IMD3 suppression. Simulation results indicate that the best 'compromise' transfer function targeting the best overall suppression also coincides with that of the upper tone. The results suggest that the F(s) transfer function should be implemented primarily between 1 and 200 MHz where the IMD3 suppression is greatest. Conveniently, the required attenuation and phase response mirrors that of a high-pass filter indicating that this transfer function is likely to be realisable.

4 | BASEBAND FEEDBACK NETWORK STABILITY

Since the proposed architecture introduces an explicit lowfrequency feedback structure in the PA, its stability must be analysed to verify that the feedback path for IMD3 suppression will not induce oscillations. The presence of a low frequency feedback path around a PA does not necessarily destabilise the circuit, and in fact can be used as a stabilisation mechanism at the frequencies where the feedback path is present [35]. In this work, the PA is first stabilised following standard RF techniques with a parallel RC network at the gate to ensure unconditional stability in the conventional shorted-baseband design case. Loop gain analysis is then applied to the network including the baseband feedback structure. The response is considered over a 100 kHz – 6 GHz frequency range, that is up to the f_{max} of the device. Both of the ideal transfer functions, minimising either the upper or lower IMD3 tone, found in Section 3, are assumed in turn. In each case, the RF input and

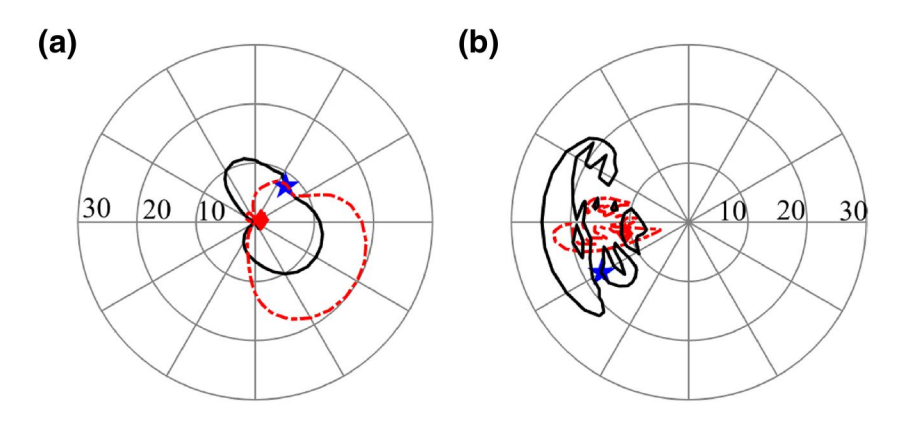
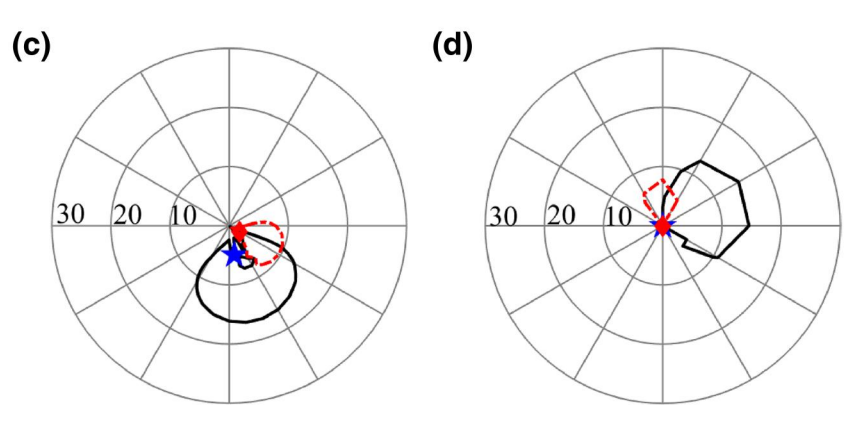


FIGURE 4 Contours of suppressed IMD3 from simulation as a function of F(s) attenuation and phase shift, represented in a polar form. Regions enclosed by the contours are regions of the F(s) plane for which the upper (red, dotted) and lower (black, solid) IMD3 is suppressed relative to the shorted baseband case. The diamond and star markers indicate a minima in the upper and lower tones, respectively. (a) 1 MHz (b) 10 MHz. (c) 100 MHz (d) 200 MHz



output terminating impedances are swept over phase with a 0.99 magnitude reflection coefficient.

Figure 6(a) and 6(b) display the loop gain envelope with the F(s), thus minimising the upper tone and lower tone, respectively. It can be seen that in both cases that the (1, 0) point in the complex plane is not encircled, indicating stability. While the envelope does closely approach the critical point in both cases, it is noted that this simulation represents a conservative estimate. In the loop gain analysis, the feedback transfer functions are assumed lossless; practical implementation will overall attenuate the response and provide a greater margin. Additionally, the closest envelopes to the (1, 0) point correspond to the load and source impedances that simultaneously have high VSWR compared to the expected 50- Ω case. In this work, it is assumed that the PA is terminated by a broadband 50- Ω load. Because the baseband feedback transfer function can be well controlled due to its low frequency and the relatively high component value precision of available inductors and capacitors in the required range, it is expected that the implemented network will not exceed the worst-case analysis shown here.

5 | IMPLEMENTATION

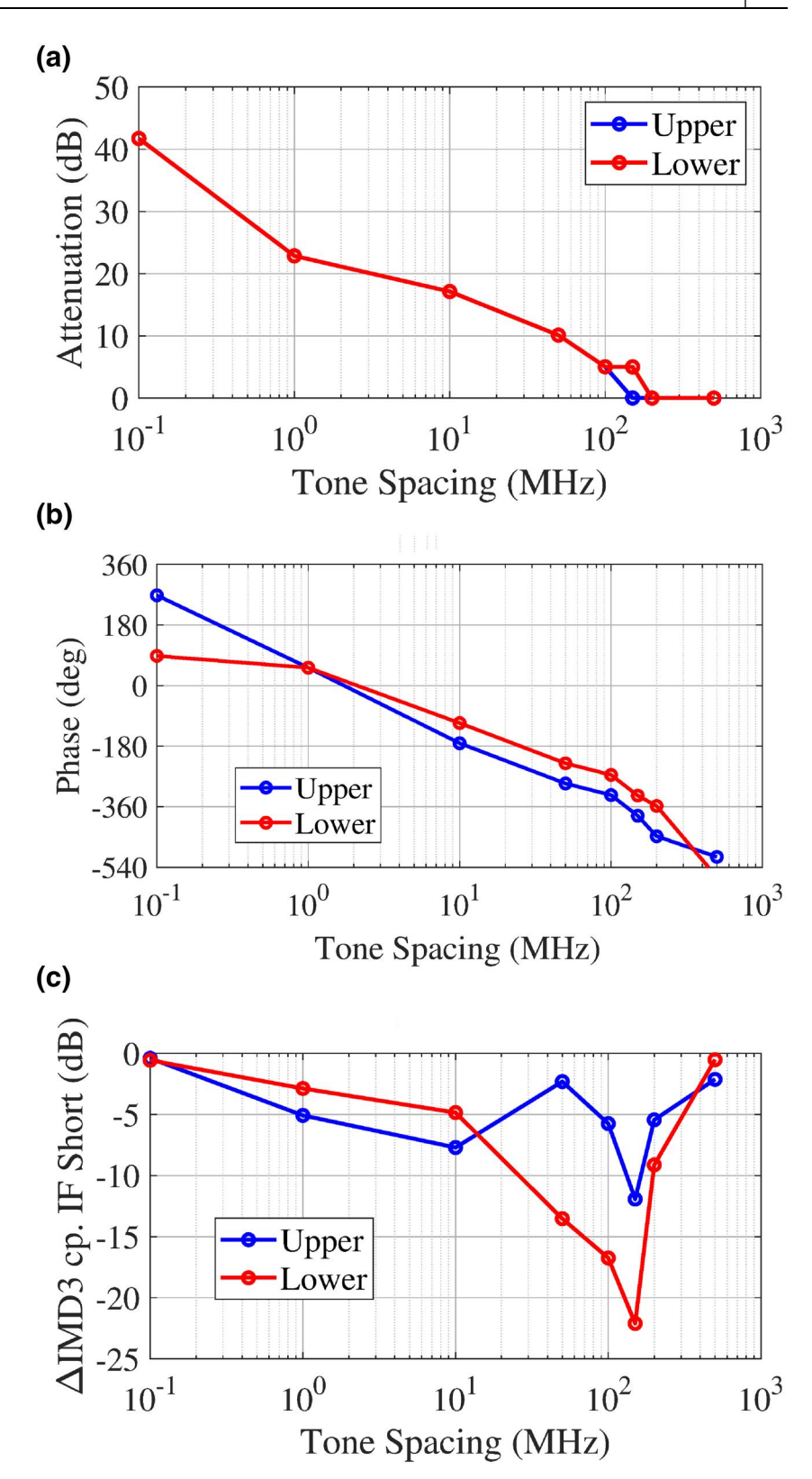
5.1 | Amplifier design

To demonstrate the proposed approach, a prototype single-ended class-AB amplifier based on the CGH270015 F 15W

GaN HEMT from Wolfspeed was designed. The transistor is biased in class AB ($I_Q = 150$ mA). This PA also serves as the basis for the simulations above used to determine the transfer functions F(s) that suppress the IMD3 tones as described in Section 3.

The layout block diagram of the designed amplifier is shown in Figure 7(a), in which both the PA design and location for the feedback transfer function can be seen. Figure 7(b) shows the output impedance targets at the fundamental and second harmonics for the class-AB amplifier based on largesignal load-pull simulation, along with the impedances presented by the output matching network (OMN). The OMN is implemented using a double-stub network to enable the straightforward impedance tuning of the fundamental and second harmonic. It can be seen that in the fundamental and second harmonic frequencies the impedances are well-matched to within 10% of their target values, but it is important to note that they are only controlled over a narrow bandwidth as the double-stub matching network precludes a wide bandwidth RF match. The quarter-wave transmission line biasing structure is placed after the OMN to ensure that different feedback network realisations do not affect the RF match to the amplifier, enabling direct comparison of performance. Similarly, the design ensures that the same placement of C_{RF} can be used for each experimental case. It has to be noted that avoiding perturbation of the second harmonic is especially critical; as described in Section 3, the second harmonic impedance determines the transfer function required to minimise IMD3.

FIGURE 5 Target feedback transfer function minimising upper (blue) and lower (red) IMD3 tones. (a) Amplitude response. (b) phase response. (c) Resulting simulated IMD3 compared with the shorted-baseband case



5.2 | Feedback network

The ideal feedback transfer function reported in Figure 5 suggests that F(s) should be implemented as a high-pass filter.

The highpass filter-like response is convenient as it can be constructed as an LC ladder network which, when implemented shunt element first, provides a biasing inductor and a dc blocking capacitor for both the gate and drain. To

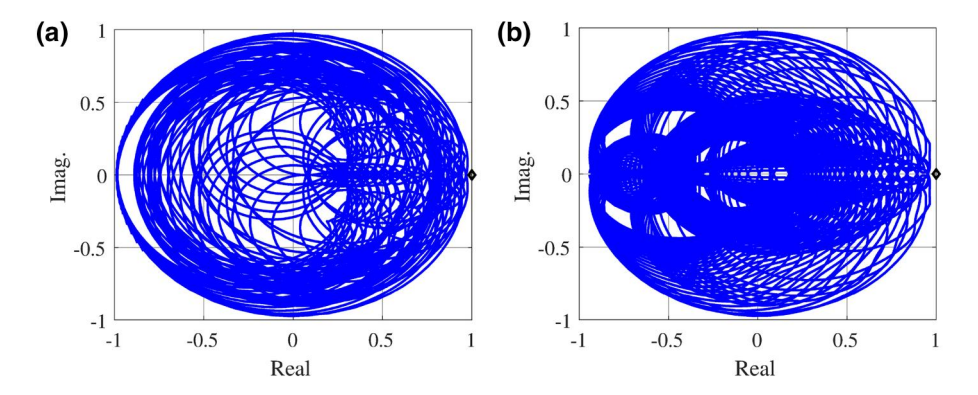


FIGURE 6 Simulated loop gain in feedback from 100 kHz to 5 GHz for (a) F(s) minimising upper IMD3 tone and (b) F(s) minimising lower IMD3 tone

experimentally demonstrate the proposed technique, both transfer functions found in Section 3, that is minimising the upper IMD3 tone (which also produces best overall suppression), and minimising the lower IMD3 tone are implemented. Suppression in the 10-100 MHz tone spacing frequency range is specifically targeted for the filter design. Beyond this frequency range, a steep increase in the required negative phase contribution from F(s) precludes practical implementation. This phase response is likely due to the practical biasing structure that was assumed in simulation.

The network in Figure 8(a) is used to implement the F(s) minimising the upper IMD3 tone. Because of the shunt-first topology, the drain and gate biases can be fed through the two inductors at either end of the network (here, the 5.8 and 3.3 μ H inductors). It is noted that these relatively large inductor values may induce undesirable self-modulation effects; a possible solution is to constrain the range of values allowed for these key components.

Filter component values are found by generating an equivalent driving-point function that corresponds to the desired filter response and then applying Cauer's second form of network synthesis [36]. A 7-pole filter found in this analysis is found to be the minimum number of poles needed to reach the total phase shift and minimise the deviation from the ideal filter trajectory between 10 and 100 MHz. The chosen values realise the measured filter response shown in Figure 9(a). In general, the transfer function is expected to elicit best performance for tone spacings around 10 MHz, or between 50 and 100 MHz.

The filter that accomplishes the lower IMD3 tone minimum is realized as shown in Figure 8(b) with five inductors and four capacitors. This filter is designed with the same procedure used to synthesise the 7-pole network. Because of the greater phase shift required for this transfer function, which precludes the 7-pole implementation, a 9-pole filter is used. An 8-pole solution is not selected as it would eliminate the shunt-L, and series-C structure that form the bias structure of the PA. As seen in Figure 9(b), the filter realizes the desired amplitude and phase response for frequencies between 10 and 100 MHz.

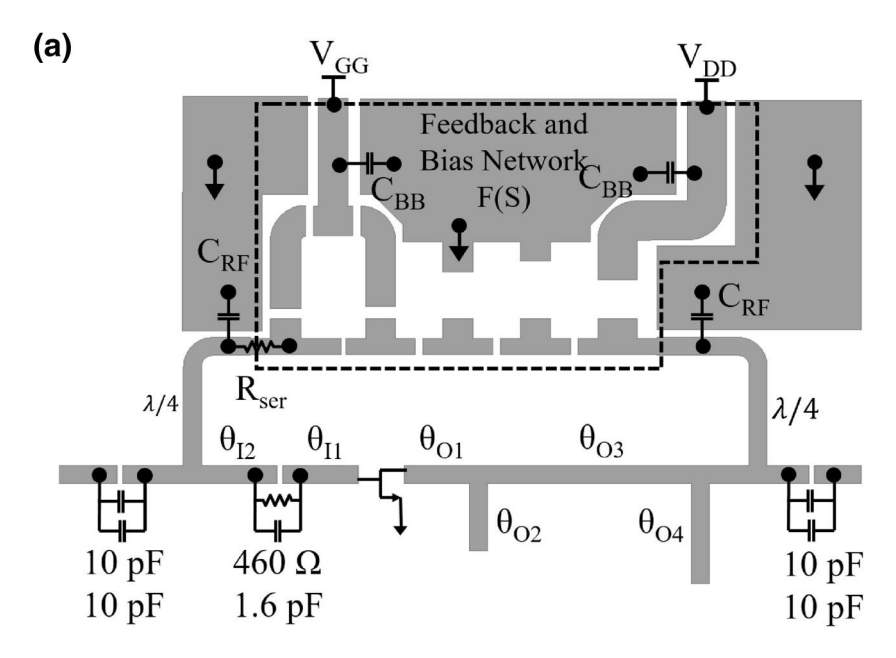
6 | MEASUREMENTS

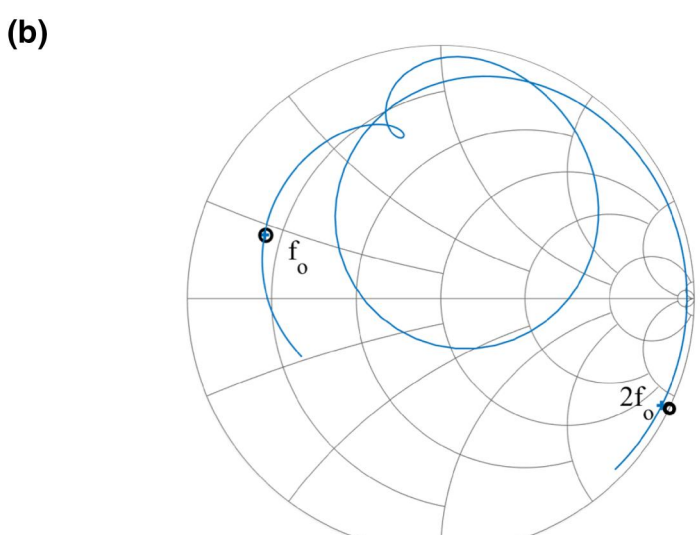
The 2.14-GHz class-AB PA described in Section 5 was fabricated on Rogers 4350B with a dielectric constant of 3.48 and a thickness of 0.03 inches. A single amplifier printed circuit board (PCB) was fabricated, including component mounting pads able to accommodate both seven pole (UTO) and nine pole (LTO) feedback variants. By re-using the same PCB, performance difference due to manufacturing and device variation is avoided. Figure 10 shows the 66 mm by 114 mm PA when populated with the 7-pole and 9-pole filters. In addition to these configurations, the PA is also characterised under the nominal shorted-baseband case, that is with the filter networks removed and the baseband termination capacitor C_{IF} included as in Figure 7 with an additional 2.2 μ F capacitor to provide a good, wideband low frequency short. The prototype is measured under CW, multitone, and complex signal excitations using the experimental setup shown in Figure 11.

6.1 CW measured performance

The PA is characterised under CW excitation when configured with a shorted baseband, 9-pole lower tone optimising (LTO), and 7-pole upper tone optimising (UTO) feedback networks. The gain and PAE versus output power for a CW power sweep at the 2.14 GHz design centre frequency is reported in Figure 12, and the response across RF frequency is reported in Figure 13. The shorted-baseband performance closely matches the predicted PAE and output power from simulation, while an approximately 1-dB gain degradation is observed which matches the prior experience with this family of devices [37]. The prototype under UTO feedback also exhibits increased PAE at 2.14 GHz compared with the shorted-baseband case while achieving the same maximum output power. The different compression points and behaviours of the three cases are attributed to channel the current non-linearities which affect the power levels at which the clipping effects dominate the gain response [38].

FIGURE 7 Prototype PA design. (a) Layout block diagram. (b) Impedance trajectory presented to the drain (cross, line) compared to target impedances (circles)





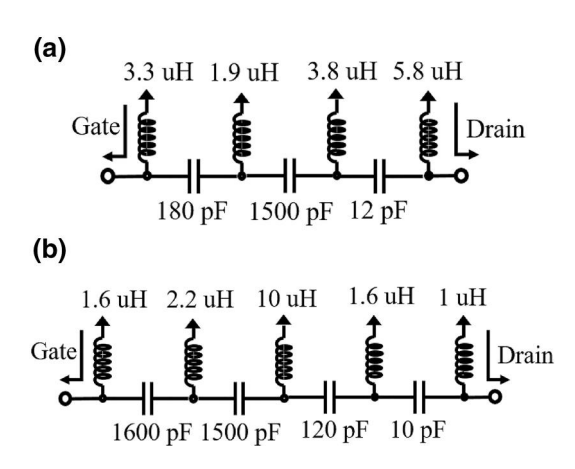
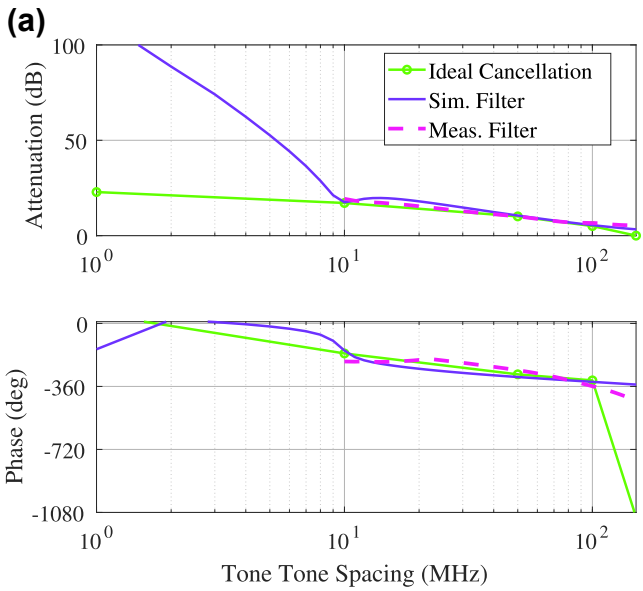


FIGURE 8 Filter Design for *F*(*s*) implementation. (a) 7-pole design realizing transfer function for upper IMD3 tone optimisation (UTO). (b) 9-pole filter for lower IMD3 tone optimisation (LTO)

6.2 | Two-tone measured performance

The experimental test setup shown in Figure 11 is used to characterise the PA response under two-tone excitation. The Rohde & Schwarz SMW200 A vector signal generator is capable of generating a clean two-tone signal and the AR 60S1G3 driver has high linearity over the range of input power levels needed by the prototype. Tone spacings between 100 kHz and 200 MHz are evaluated. The measurements presented here compare the two feedback filter designs to the nominal case, that is shorted-baseband. In these comparisons, IMD3 suppression is presented as the difference between IMD3 of the feedback case to the baseband short, that is negative Δ IMD3 in the following plots corresponds to an improvement in IMD3 suppression.

Figure 14(a) reports the IMD3 measured for the shorted-IF, UTO filter, and LTO filter cases, and Figure 14(b) reports



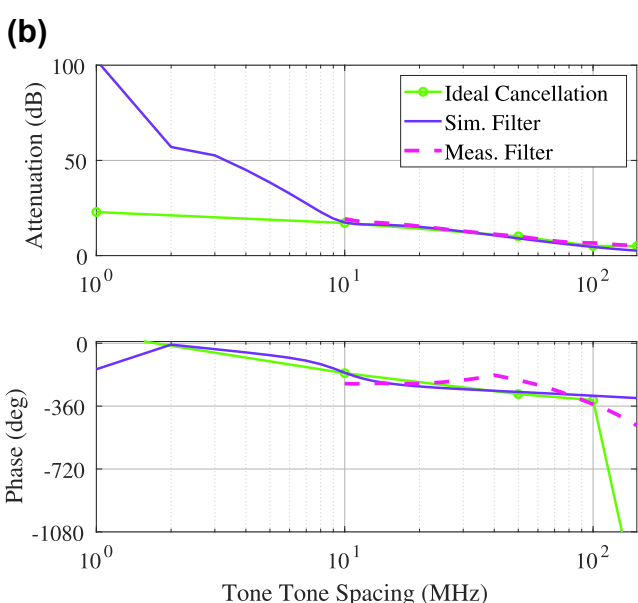


FIGURE 9 Measured feedback network response for minimisation of (a) upper tone optimising (7-pole filter) and (b) lower tone optimising (9-pole filter). Measured results are restricted to frequencies greater than 10 MHz due to the limitations of available measurement equipment, but all frequencies over which the feedback is designed to operate is covered

the IMD3 suppression of each feedback topology relative to the shorted IF case. The UTO filter evidently provides a better response across power levels, with the LTO filter degrading IMD3 in back-off and at the P3dB design power only suppressing the lower tone. A similar trend is seen in Figure 15, where the UTO filter provides better suppression over the majority of the tone spacing frequency range at 42.5 dBm output power (P3dB of the no feedback response).

Over a 1-MHz to 200-MHz range, both IMD3 tones are suppressed relative to the nominal shorted-baseband case, with maximum suppression occurring at the target design frequency of 10 MHz. When compared with the simulated IMD3

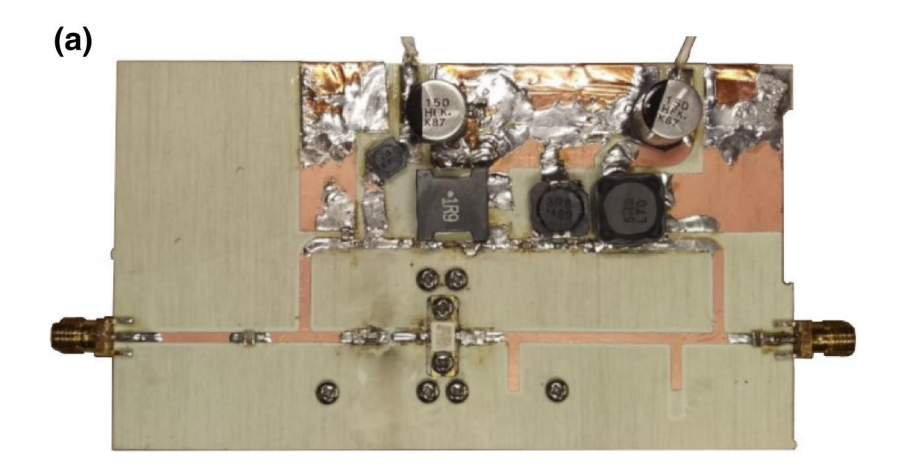
suppression in Figure 5, baseband frequencies above 10 MHz under UTO feedback show suppression relative to the no feedback case, but the suppression is much lower than predicted in simulation. The measured results show the best case suppression of -9 dB at 10 MHz, compared with the expected -23 dB at 150 MHz. This difference between simulation and measurement is related to the imperfect realisation of the required transfer functions [Figure 5] by the filter, and to inaccuracies in the large-signal model in predicting the optimal baseband terminations. This result indicates that experimentally determining the amplitude and phase response across frequency for F(s) might lead to further improvements in performance over the full baseband frequency range shown, an action that was not taken in this work. Nonetheless, the technique appears promising and either maintains or improves the IMD3 performance of the amplifier compared with the nominal case without perturbing the RF performance.

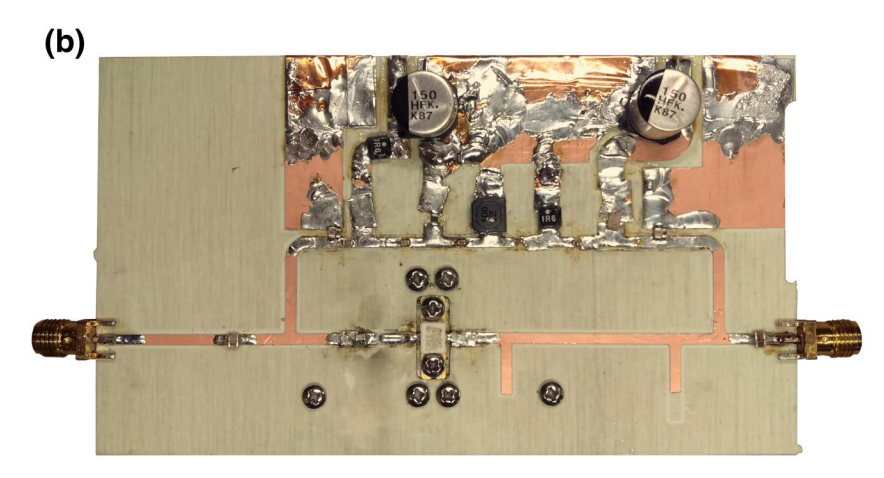
6.3 | Complex signal measured performance

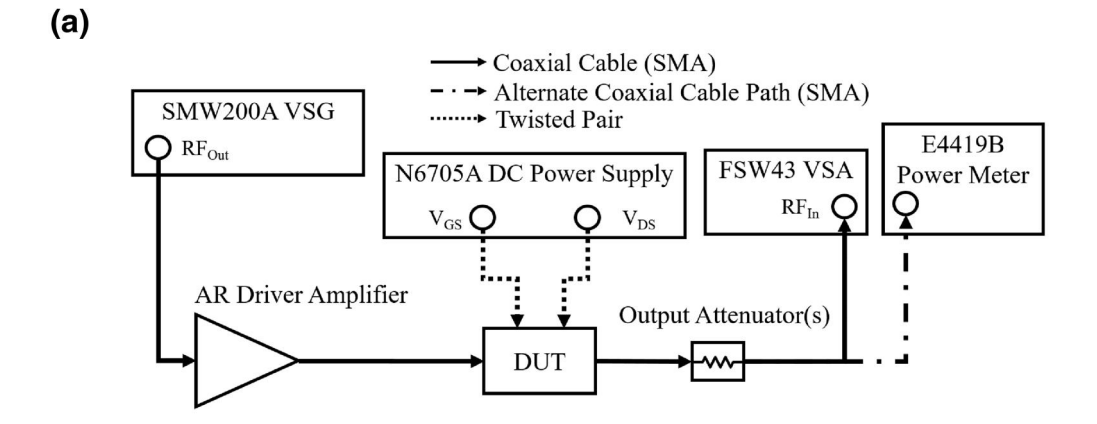
Although the proposed technique is designed based on twotone simulations, the performance for complex modulated signals is also evaluated. No digital predistortion is applied to any of the following measurements. The amplifier with the UTO feedback network and no feedback network are evaluated when excited by a 30-MHz wide carrier-aggregated 64QAM LTE signal with three 10-MHz component carriers centred at 2.14 GHz, with a measured 12.8-dB overall PAPR. The measured output power is 29.1 dBm with 16.5% drain efficiency. The resulting amplifier output spectrums are compared in Figure 16a. The benefits of the UTO feedback network are present within the inter-component carrier guard bands and in the initial out-of-band (OOB) regions of the spectrum are observed.

The UTO network realizes a 6-8 dB suppression in the power spectral density of the inter-component carrier guard bands compared with the conventional amplifier design without the feedback. In the critical out-of-band (OOB) region specified by the LTE standard extending 25 MHz from either end of the signal [39], the UTO feedback network suppresses the power spectral density by 2-3 dB without any measurable difference in the gain or drain efficiency of the amplifier. Next, the out of band response of the two networks at 80-MHz and 400-MHz offset duplex frequencies is characterised from the 30 MHz wide modulated signal. At the below-band 80-MHz offset duplex frequency from the transmission band, the UTO network realises a 46% reduction in output power over a 30-MHz bandwidth compared with the amplifier without feedback. At the above-band 80-MHz offset frequency, the UTO network realises a 33% output power reduction over a 30-MHz bandwidth compared with the amplifier without feedback. At the below-band and above-band 400-MHz offset duplex frequency, the UTO network realises an identical output power over a 30-MHz bandwidth compared with the amplifier without the feedback. These results demonstrate that the

FIGURE 10 Photograph of the fabricated amplifier with feedback networks for (a) UTO (7 poles) and (b) LTO (9 poles)









 $FIGURE\ 11\quad \text{Measurement test bench (a) Block diagram and (b) Photograph}$

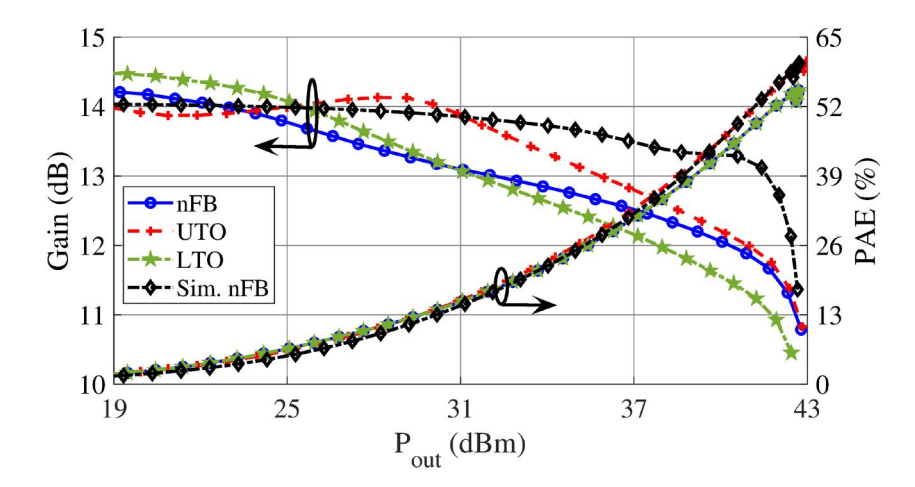


FIGURE 12 CW response with (UTO, LTO) and without (nFB) feedback under CW excitation at the nominal 2.14 GHz design frequency compared with the no feedback case in simulation

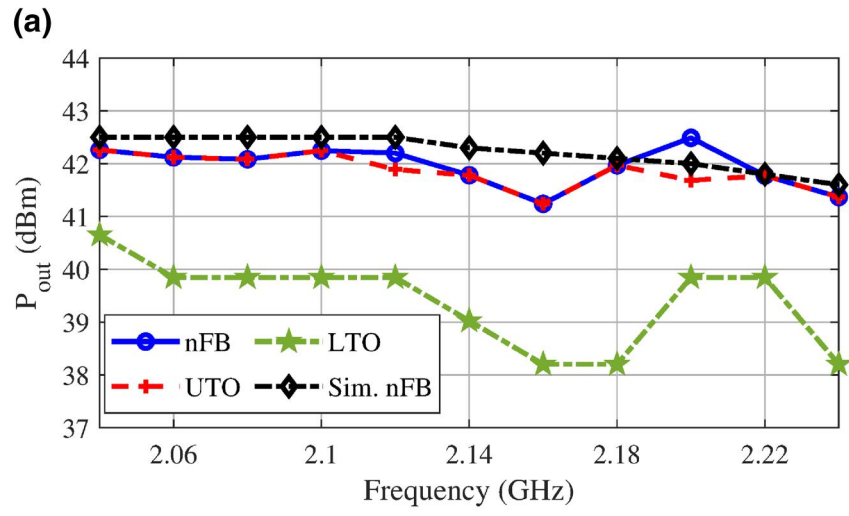
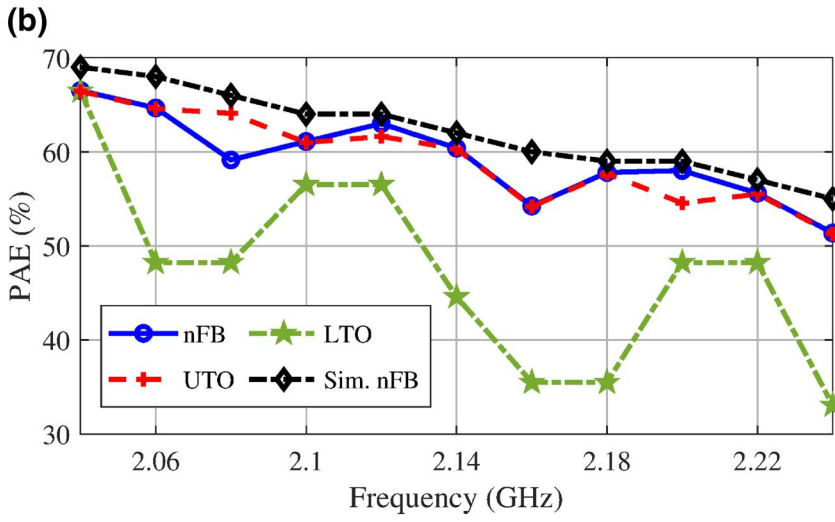


FIGURE 13 CW frequency response with (UTO, LTO) and without (nFB) feedback.
(a) Output power at P3dB. (b) PAE at P3dB. Simulation results are for the no feedback (nFB) case

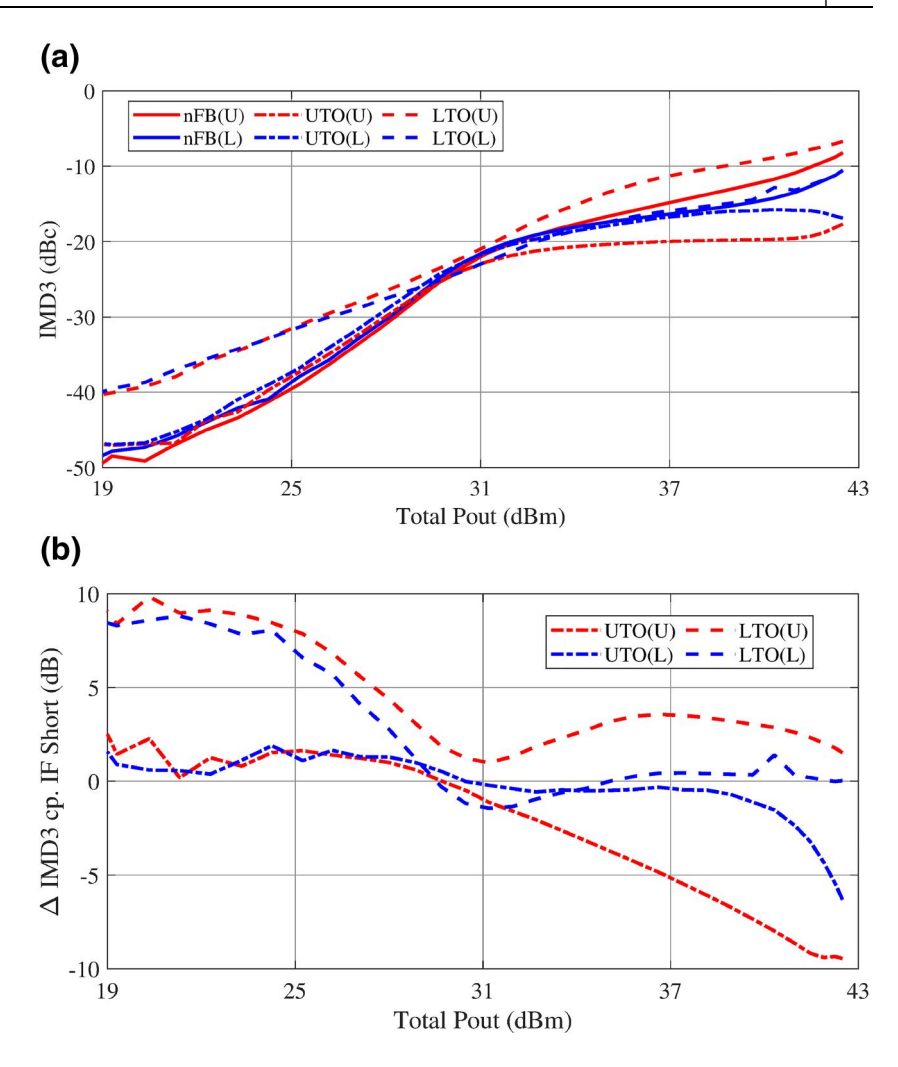


feedback network suppresses distortion products immediately outside of the transmit signal band without worsening the further out of band response of the amplifier.

Both networks are compared on the basis of signal error vector magnitude (EVM) using the Rhode and Schwarz SMW200 A and FSW43-K18 EVM measurement option. The

following results include the effect of the ZVE-3W-83+ driver amplifier on the modulated signal and are reported to the precision given by the instrumentation. The UTO feedback network realizes a mean raw EVM of 19.660% and max raw EVM of 168.065% compared with the no feedback network which realizes a modulated mean raw EVM of 19.858% and

FIGURE 14 Measured IMD3 over power at a 10-MHz tone spacing. (a) Comparison of performance without feedback and with the LTO and UTO feedback networks. (b) IMD3 difference in feedback compared with the shorted-baseband termination (nFB from (a))



max raw EVM of 176.113%. The UTO feedback network realizes a 0.198 percentage point mean raw EVM improvement and an 8.048 percentage point max raw EVM improvement at the same peak output power level. The low improvement in mean raw EVM and larger improvement in max raw EVM is consistent with the selection of the P3dB point for optimization of the UTO feedback network as the max raw EVM is driven by the distortion behaviour of the amplifier in deep compression, where this feedback loop is optimised to suppress distortion. Improvement of the mean raw EVM can befurther improved through re-optimisation of the feedback network to realise greater suppression in backoff compared with the current design.

Next, the amplifier with the UTO feedback network and no feedback is evaluated when excited by a 200-MHz wide carrier-aggregated 64QAM LTE signal made up of ten 20-MHz component carriers centred at the amplifier centre frequency of 2.14 GHz, with a measured 9.2-dB overall PAPR. The measured output power is 33.3 dBm with 16.6% drain efficiency. The resulting amplifier output spectrums are compared in Figure 16b. This measurement displays significant gain variation of this PA across the band (on the order of 5 dB) for the amplifier with and without feedback present.

Minimising this response was not an immediate focus of this work. In the guard bands between the 20-MHz component carriers, the UTO feedback network realises a 4-5 dB suppression in power spectral density, smaller than the 6-8 dB suppression observed in the 30-MHz case. In the OOB region below the 200-MHz signal, the UTO network realises a consistent 2-4 dB suppression in the power spectral density. The EUTRA specification calls for a -21 dB suppression within the OOB region, which the amplifier with the UTO feedback network achieves while the amplifier without feedback does not. At the below-band 80-MHz offset duplex frequency from the transmission band the UTO network realises a 30% reduction in output power over a 200 MHz bandwidth compared with the amplifier without feedback. At the aboveband 80-MHz offset frequency, the UTO network realises a 20% output power reduction over a 200 MHz bandwidth compared with the amplifier without feedback. At the belowband 400-MHz offset duplex frequency, the UTO network realises an identical output power over a 200 MHz bandwidth compared with the amplifier without feedback. At the aboveband 400-MHz offset duplex frequency, the UTO network realises a 20% reduction in output power over a 200 MHz bandwidth compared with the amplifier without feedback.

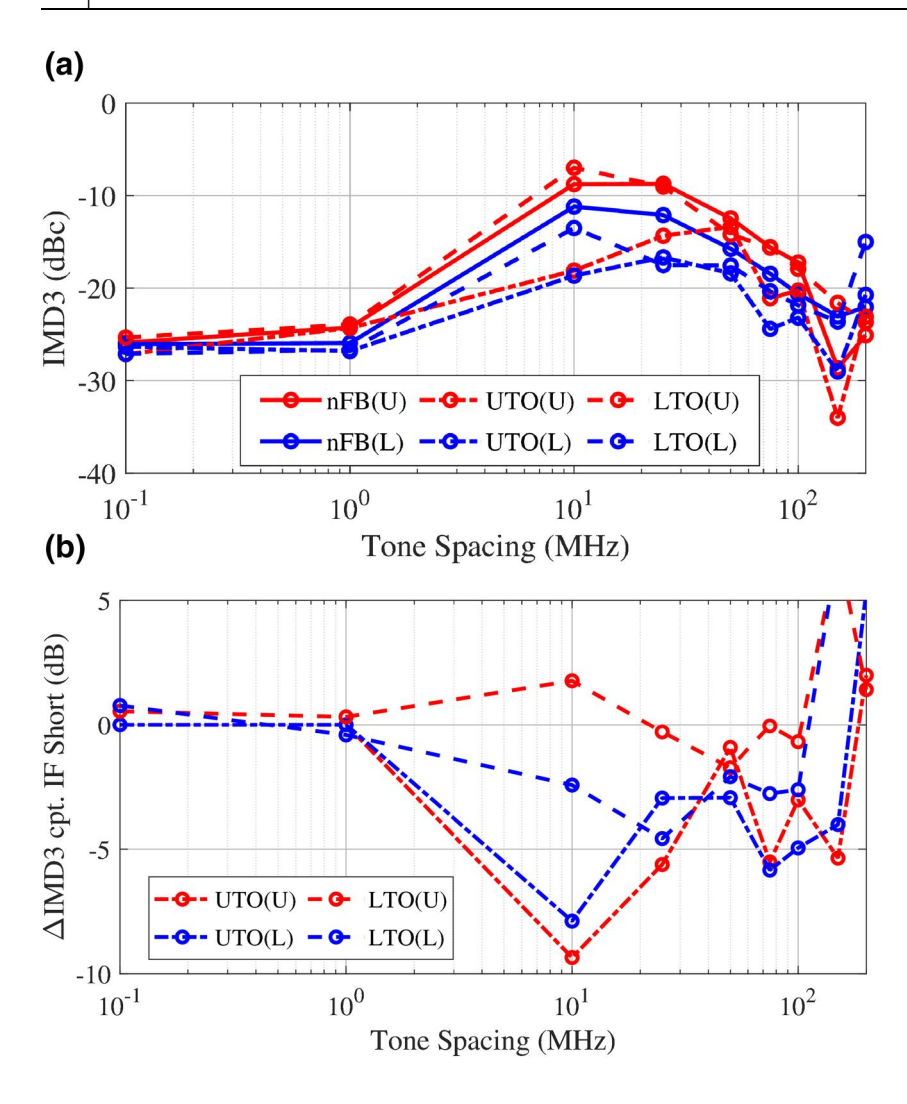


FIGURE 15 IMD3 at of each network at 42.5 dBm output power (P3dB of the no feedback response) measured across the frequency.
(a) Comparison of performance without feedback and with the LTO) and UTO feedback networks.
(b) IMD3 difference in feedback compared with the shorted-baseband termination

These results demonstrate that the feedback network suppresses distortion products immediately outside the transmit signal band without worsening further the out of band response of the amplifier.

The UTO feedback network with 200-MHz wide signal excitation realizes a modulated mean raw EVM of 24.434% and max raw EVM of 144.033% compared with the no feedback network which realizes a modulated mean raw EVM of 20.722% and max raw EVM of 185.535%. The UTO feedback network realizes a 3.712 percentage point mean raw EVM degradation and a 41.15 percentage point max raw EVM improvement at the same peak output power level. The degradation of mean raw EVM can be attributed to the limited distortion suppression in backoff exhibited by the UTO feedback network, although the network could be adjusted based on modulated measurements to realise better EVM compared with the current design. Similar to the 30-MHz case, the larger improvement in max raw EVM is consistent with the selection of the P3dB point for optimization of the UTO feedback network as the max raw EVM is driven by the distortion behaviour of the amplifier in deep compression, where this feedback loop is optimised to suppress distortion. As in the 30-MHz signal case, the amplifier's gain and drain efficiency is not affected.

The UTO feedback network helps to linearise the amplifier response compared with the no feedback case, but the benefits of that linearisation are reduced when compared with the two-tone test cases. There are several non-linear effects associated with the greater modulation complexity of the LTE signal compared to a two-tone excitation. The most notable change in complexity is the presence of intertone phasing effects, which are not present in the two tone case [28, 34, 38, 40]. Furthermore under LTE excitation, the effects of fundamental-frequency and harmonic impedance terminations on performance (e.g., gain flatness) have a pronounced effect not controlled through baseband feedback. Likewise, the proposed technique does not compensate for trapping and thermal effects. It is also important to note that the limited IMD3 suppression in power backoff under UTO feedback, as shown in Figure 14, will mean the LTE signal will realize smaller distortion suppression compared with the max -9 dB due to the high signal PAPR.

Nonetheless, these preliminary results indicate the benefits of the proposed feedback technique.

A summary of performance and comparison to related techniques in analogue linearisation is given in Table 1.

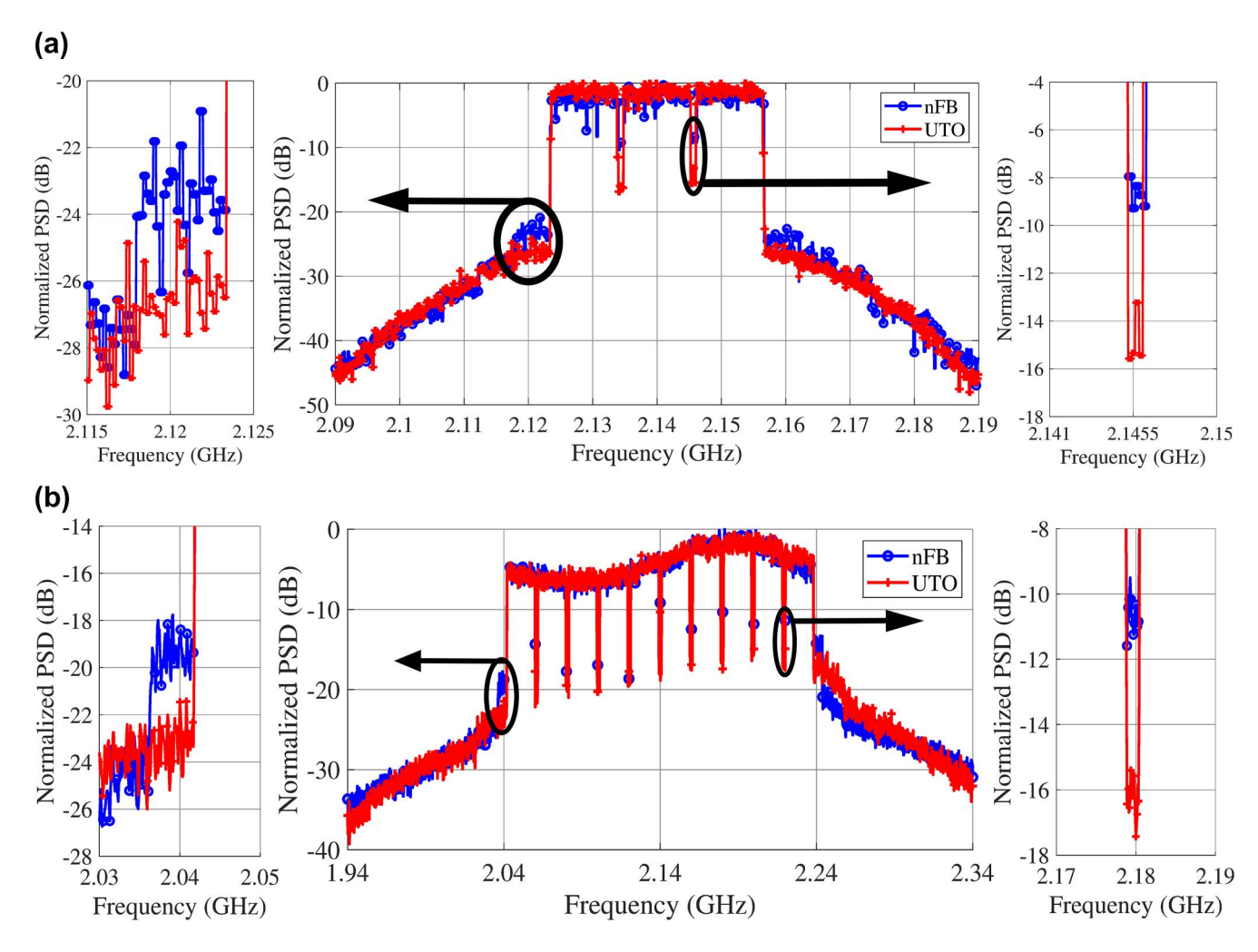


FIGURE 16 Output spectrum of a carrier aggregated 64QAM LTE signal with (a) three component carriers each of 10 MHz bandwidth with and without baseband feedback at peak envelope power of P3dB and (b) a carrier aggregated LTE signal with 10 component carriers each of 20 MHz bandwidth with and without baseband feedback at peak envelope power of P3dB. Details of a guard band between component carriers and the lower OOB band are shown. All devices are normalized to the peak output power of the no feedback case

TABLE 1 Comparison of RF performance to analogue distortion reduction techniques

	Tech.	Architecture	Amp. Elements	Freq. (GHz)	P _{out} (dBm) @ P3dB	PAE (%) @ P3dB	Two-Tone @ P3dB		
Ref.							IMD3 (dBc)	Improvement (dB)	Spacing (MHz)
[7]	*	Feedforward	2	8.15	0		-63.6	18	500
[41]	GaN	Transistor APD	3	2.4	38.9	43	-35	10	10
[42]	*	Polar Env. F.B.	1	1.8	31	*	-47.02	15.19	1
[9]	0.15um	IM2	2	24	21	*	-4 0	3.7	1
	PHEMT	Feedforward							
[15]	GaN	Sweet spot	1	3	33	45	-25	*	5
[43]	GaN	Doherty	1	5	37	60	-45	*	2.5
[10]	*	Diode linearizer	1	0.5	53	*	6 MHz OFDM U1/L1: -32 dBc/-32 dBc		
[11]	*	Diode linearizer	1	2.7	34.1	37.9	28.6 kHz CDMA U1/L1: -36.7 dBc/-36.7 dBc		
[31]	GaN	IF feedback	1	0.85	41	48	-25	9	5
This work	GaN	IF feedback	1	2.14	42.5	59	-2 0	0.5	1

Note: * - not reported.

Although direct comparisons are difficult, significant improvements in IMD3 tend to correspond to architectures employing multiple active devices, for example [7]. It is also noted that the majority of techniques address narrow tone spacings or narrowband modulated signals. The relatively high efficiency of the baseband feedback approach can be attributed to it not requiring insertion of any elements in the RF path. As it can be seen from this comparison, the proof-of-concept baseband feedback demonstration offers IMD3 suppression with only modest increase in circuit complexity, and no effective operating difference at the system level.

7 | CONCLUSION

The baseband feedback approach presented in this article offers a practical implementation of negative baseband impedance synthesis for IMD3 suppression. The 2.14-GHz proof-of-concept prototype is implemented using hybrid PA design techniques and has 14.8 dB small-signal gain and a peak PAE of 60.1%. The implemented feedback structure demonstrates suppression of IMD3 tones at P3dB for tone spacing up to 200 MHz, with nearly 10% of the RF carrier frequency, relative to the nominal case without the feedback. In preliminary tests with modulated signals, the feedback structure demonstrates an improved ACLR and EVM, although further investigation is needed.

The proposed approach centres on controlling the amplitude and phase of the feedback path connecting the drain and gate biases. Compared with the previous work [31], the technique has been shown to simultaneously suppress both the upper and lower IMD3 tones, and over a wide range of tone spacing. Suppression at P3dB is targeted in this work due to the challenges of linearisation at this power level through other means such as sweet-spot design. The capability to suppress the IMD3 in gain compression prevents the need to operate the PA in back-off, thus allowing for higher power and higher efficiency operation. Although only this specific power level is designed, IMD3 suppression is observed over a range of power levels in measurement. This result implies that an experimental determination of the feedback transfer function (rather than relying on a simulation model not designed for this application) may lead to further improvements. Furthermore, designing for a lower power level may be advantageous for suppression over a wider power range. The technique is expected to scale to higher carrier frequencies, where wider absolute instantaneous bandwidths pose a challenge for DPD, offering a potential path to augment the DPD techniques.

ACKNOWLEDGEMENT

This material is based on the work supported by the National Science Foundation under Grant No. 1,846,507. The authors would like to acknowledge Qorvo, Inc. for the loan of the Amplifier Research 60S1G3 driver amplifier used in this work, and Rohde & Schwarz USA for the loan of the FSW43 Signal and Spectrum Analyser.

ORCID

William Sear https://orcid.org/0000-0003-3037-2641
Taylor W. Barton https://orcid.org/0000-0001-6962-0740

REFERENCES

- Tripathi, G.C., Rawat, M.: RF in RF out linearizer system design for satellite communication. IEEE Trans Electron Dev. 65(6), 2378–2384 (2018)
- Lasser, G., Duffy, M.R., Popović, Z.: Dynamic dual-gate bias modulation for linearisation of a high-efficiency multistage PA. IEEE Trans Microw Theory Techn. 67(7), 2483

 –2494 (2019)
- Pan, W., et al.: Digital linearisation of multiple power amplifiers in phased arrays for 5G wireless communications. In: IEEE International Symposium on signal Processing and information Technology, pp. 247–251 (2018)
- Hesami, S., et al.: Single digital predistortion technique for phased array linearisation. In: IEEE International Symposium on circuits and systems, pp. 1–5 (2019)
- Liu, X., et al.: Beam-oriented digital predistortion for 5G massive MIMO hybrid beamforming transmitters. IEEE Trans Microw Theory Techn. 66(7), 3419–3432 (2018)
- Katz, A., Wood, J., Chokola, D.: The evolution of PA linearisation: from classic feedforward and feedback through analog and digital predistortion. IEEE Microw Mag. 17(2), 32–40 (2016)
- Hickson, M.T., et al.: High efficiency feedforward linearizers European Microwave Conference, vol. 1, pp. 819–824 (1994)
- Horiguchi, K., et al.: A high efficiency feedforward amplifier with a series diode linearizer for cellular base stations. IEEE International Microwave Sympsoium Digest. vol. 2, 797–800 (2001)
- Chen, Y.H., et al.: A 24 GHz CMOS power amplifier with successive IM2 feed-forward IMD3 cancelation. In: IEEE International microwave Symposium, pp. 1–4 (2015)
- Yamauchi, K., et al.: Series anti-parallel diode linearizer for class-B power amplifiers with a gain expansion. In: Asia-pacific microwave Conference, pp. 883–886 (2006)
- Yamauchi, K., et al.: A microwave miniaturised linearizer using a parallel diode with a bias feed resistance. IEEE Trans Microw Theory Techn. 45(12), 2431–2435 (1997)
- Bera, S.C., et al.: Temperature behaviour and compensation of diodebased pre-distortion linearizer. IEEE Microw Wireless Compon Lett. 23(4), 211–213 (2013)
- Hu, X., et al.: Predistortion linearisation of an X-band TWTA for communications applications. IEEE Trans Electron Dev. 58(6), 1768–1774 (2011)
- Park, B., et al.: Highly linear mm-wave CMOS power amplifier. IEEE Trans Microw Theory Techn. 64(12), 4535–4544 (2016)
- de Falco, P.E., Birchall, J., Smith, L.: Hitting the sweet spot: a single-ended power amplifier exploiting class AB sweet spots and optimised third harmonic termination. IEEE Microw Mag. 18(1), 63–70 (2017)
- Fager, C., et al.: A comprehensive analysis of IMD behaviour in RF CMOS power amplifiers. IEEE J Solid-State Circuits. 39(1), 24–34 (2004)
- Lavrador, P.M., et al.: The linearity-efficiency compromise. IEEE Microw Mag. 11(5), 44–58 (2010)
- Cripps, S.C.: Advanced techniques in RF power amplifier design. Artech House microwave library (Artech House 2002)
- Chaudhary, M.A., et al.: Optimization of out-of-band impedance environment for linearity improvements of microwave power transistors. In: International Conference on Electrical and Electronic Engineering, pp. 219–223 (2018)
- Tasker, P.J., Benedikt, J.: Waveform inspired models and the harmonic balance emulator. IEEE Microw Mag. 12(2), 38–54 (2011)
- Carvalho, N.B., Pedro, J.C.: Two-tone IMD asymmetry in microwave power amplifiers IEEE International Microwave Symposium Digest, vol. 1, pp. 445

 –448 (2000)

 Tasker, P.J.: Practical waveform engineering. IEEE Microw Mag. 10(7), 65–76 (2009)

- Hashmi, M.S., Ghannouchi, F.M., Tasker, P.J.: High frequency waveform engineering and its applications: Tutorial 54. IEEE Instrum Meas Mag. 18(3), 44–50 (2015)
- Akmal, M., et al.: The effect of baseband impedance termination on the linearity of GaN HEMTs. In: European microwave Conference, pp. 1046–1049 (2010)
- Hu, Y., Mollier, J.C., Obregon, J.: A nevv [sic] method of third-order intermodulation reduction in nonlinear microwave systems. IEEE Trans Microw Theory Techn. 34(2), 245–250 (1986)
- Brinkhoff, J., Parker, A.E.: Effect of baseband impedance on FET intermodulation. IEEE Trans Microw Theory Techn. 51(3), 1045–1051 (2003)
- Akmal, M., et al.: The effect of baseband impedance termination on the linearity of GaN HEMTs. In: European microwave Conference, pp. 1046–1049 (2010)
- de Carvalho, N.B., Pedro, J.C.: A comprehensive explanation of distortion sideband asymmetries. IEEE Trans Microw Theory Techn. 50(9), 2090–2101 (2002)
- Carrubba, V., et al.: Class-BJ power amplifier modes: the IMD behaviour of reactive terminations. In: European microwave Conference, pp. 1391– 1394 (2013)
- Armstrong, E.H.: The super-heterodyne-its origin, development, and some recent improvements. Proc Inst Radio Eng. 12(5), 539–552 (1924)
- Sear, W., Barton, T.W.: A baseband feedback approach to linearisation of a uhf power amplifier. In: 2019 IEEE MTT-S International microwave Symposium (IMS), pp. 75–78 (2019)
- Pedro, J.C., et al.: A new power amplifier behavioural model for simultaneous linearity and efficiency calculations. In: 2012 IEEE/MTT-S International microwave Symposium digest, pp. 1–3 (2012)
- Roblin, P., Chang, H.: Chireix amplifier with enhanced bandwidth using active load. In: IEEE International wireless Symposium, pp. 1–4 (2018)
- Borges de Carvalho, N., Pedro, J.C.: Compact formulas to relate ACPR and NPR to two-tone IMR and IP3. Microw J (1999)

- Sear, W., Barton, T.W.: Power-amplifier stabilisation through out-ofband feedback. IEEE Microw Wireless Compon Lett. 30(8), 768–771 (2020)
- Lam, H.Y.F.: Analog and digital filters: design and Realization, 1st ed. Prentice Hall (1979)
- Pednekar, P.H., et al.: Analysis and design of a Doherty-like rf-input load modulated balanced amplifier. IEEE Trans Microw Theor Tech. 66(12), 5322–5335 (2018)
- Cabral, P.M., Pedro, J.C., Carvalho, N.B.: Bias networks impact on the dynamic am/am contours in microwave power amplifiers. In: 2006 International Workshop on Integrated Nonlinear Microwave and Millimetre-wave circuits, pp. 38–41 (2006)
- 3GPP: Evolved Universal Terrestrial Radio access (E-UTRA); user equipment (UE) radio transmission and reception. (3rd Generation Partnership Project (3GPP)). 36.331. version 14.3.0 (2017)
- Pedro, J.C., Nunes, L.C., Cabral, P.M.: Soft compression and the origins of nonlinear behaviour of GaN HEMTs. In: European microwave Conference, pp. 1297–1300 (2014)
- Cai, Q., et al.: A simplified transistor-based analog predistorter for a GaN power amplifier. IEEE Transactions on Circuits and Systems II: Express Briefs. 65(3), 326–330 (2018)
- Park, H.M., et al.: A predistortion linearizer using envelope-feedback technique with simplified carrier cancelation scheme for class-A and class-AB power amplifiers. IEEE Trans Microw Theory Techn. 48(6), 898–904 (2000)
- Musolff, C., Kamper, M., Fischer, G.: Linear Doherty PA at 5 GHz. IEEE Microw Mag. 16(1), 89–93 (2015)

How to cite this article: Sear W, Barton TW. Wideband IMD3 suppression through negative baseband impedance synthesis. *IET Microw. Antennas Propag.* 2021;15:728–743. https://doi.org/10.1049/mia2.12075